

Numerical investigations of traveling singular sources problems via moving mesh method

Zhicheng Hu^{a,*}, Keiwei Liang^b

^a*LMAM & School of Mathematical Sciences, Peking University, Beijing 100871, China*

^b*Department of Mathematics, Zhejiang University, Hangzhou 310027, China*

Abstract

This paper studies the numerical solution of traveling singular sources problems. In such problems, a big challenge is the sources move with different speeds, which are described by some ordinary differential equations. A predictor-corrector algorithm is presented to simulate the position of singular sources. Then a moving mesh method in conjunction with domain decomposition is derived for the underlying PDE. According to the positions of the sources, the whole domain is splitted into several subdomains, where moving mesh equations are solved respectively. On the resulting mesh, the computation of jump $[\dot{u}]$ is avoided and the discretization of the underlying PDE is reduced into only two cases. In addition, the new method has a desired second-order of the spatial convergence. Numerical examples are presented to illustrate the convergence rates and the efficiency of the method. Blow-up phenomenon is also investigated for various motions of the sources.

Keywords: Moving mesh method; Domain decomposition; Traveling singular sources

1 Introduction

We take the one-dimensional moving singular sources equation

$$u_t - u_{xx} = \sum_{i=0}^{q-1} F_i(t, x, u) \delta(x - \alpha_i(t)), \quad -\infty < x < \infty, \quad t > 0, \quad (1)$$

$$u(x, 0) = u_0(x), \quad -\infty < x < \infty, \quad (2)$$

$$u(x, t) \rightarrow 0 \quad \text{as} \quad |x| \rightarrow \infty, \quad t > 0. \quad (3)$$

as the model problem in this paper. Here $q > 0$ is the number of singular sources. The initial value $u_0(x)$ is taken to be continuous and compatible with the boundary conditions, i.e. $u_0(x) \rightarrow 0$ as $|x| \rightarrow \infty$. The local source functions $F_i(t, x, u)$ ($i = 0, 1, \dots, q-1$) might be given a priori or can be determined from some additional constraints on the solution. The traveling sources are located at

*Corresponding author.

E-mail address: huzhicheng1986@gmail.com (Z. Hu); matlkw@zju.edu.cn (K. Liang).

$\alpha_i(t)$, $i = 0, 1, \dots, q-1$. In general, their velocities can be described by several ordinary differential equations

$$\frac{d\alpha_i}{dt} = \psi_i(t, \alpha_i(t), u), \quad i = 0, 1, \dots, q-1, \quad (4)$$

which are coupled with the solution u . We assume that the sources do not intersect with each other during the time in consideration. This model arises in many areas such as laser beams traveling problems where u is the temperature of the material [1], or free-boundary solidification problems where $\alpha_i(t)$, $i = 0, 1, \dots, q-1$, are the moving interfaces between different phases [2].

It is well known that the solution of the model is continuous and piecewise smooth [3]. However, the derivative of the solution has a jump at each source due to the delta function singularity on it, and the jump is given by [4]

$$[u_x]_{(\alpha_i(t), t)} = -F_i(t, \alpha_i(t), u(\alpha_i(t), t)), \quad i = 0, 1, \dots, q-1. \quad (5)$$

This leads the standard numerical methods, either finite difference method or finite element method, might fail when crossing the time-dependent source positions. Various approaches, have been used to deal with the delta function singularity, such as the immerse boundary (IB) method and the immerse interface method (IIM) [2, 3, 5–8]. For the IB method originally proposed by [9], the delta function is approximated by an appropriately chosen discrete delta function. Beyer and LeVeque [2] studied various cases of the model (1)–(3) for the IB method with $q = 1$, and the source position $\alpha_i(t)$ being priori specified. In contrast, the IIM first introduced by LeVeque and Li [6] incorporates the known jumps of solution or its derivatives into the finite difference scheme to obtain a modified discretization scheme. Li [3] developed an IIM numerical algorithm on the uniform mesh for the model (1)–(3) and (4) with $q = 1$.

The model (1)–(3) and (4) is more difficult to be solved when the source function $F_i(t, x, u)$ is high nonlinearity. In this case, the solution is always blow-up in some finite time $T > 0$ if the sources are stationary or move at sufficiently low speed, while blow-up will be avoided if the sources move at sufficiently high speed (see e.g. [1, 10, 11]). As the solution evolves singularity, the uniform mesh method always become computationally prohibitive. Hence, moving mesh method has to be employed, which is one of the most popular adaptive methods and have been successfully used to investigate the blow-up phenomenon [12, 13]. In MMPDE's approaches, the movement of the mesh is controlled by the moving mesh partial differential equations (MMPDEs) based on the equidistribution principle [14]. Among these MMPDEs, MMPDE4, MMPDE5 and MMPDE6 are popular to use. Readers interested in the moving mesh method and its applications can refer to the books [15, 16].

Recently, several papers have been devoted to moving mesh method for the model (1)–(3) with a priori specified source position $\alpha_i(t)$ for $q = 1$ [4, 17] and for $q > 1$, in which the sources move with the same speed [18, 19]. This paper is a further study of [19] and [20] for the model (1)–(3) with general movement of the sources, which do not intersect with each other during time evolution. First, we choose a finite observed domain containing all sources with appropriate boundary conditions, and divide it into $q + 1$ subdomains by the q sources. Obviously, the sizes of the subdomains are changed as the sources traveling. MMPDEs are applied on each subdomain to obtain a local equidistributed mesh on it. Then the underlying PDE (1) is solved on the whole observed domain

with the mesh composed of the local mesh on each subdomain. Taking the advantages of domain decomposition [21], MMPDEs could be solved efficiently by parallel computing. Moreover, It can be found that the computation of $[\dot{u}]$ is avoided, thus the discretization scheme for the underlying PDE becomes very simple. In addition, our method has an expected second-order convergence in space.

The organization of the paper is as follows. In section 2, we introduce the moving mesh method in conjunction with domain decomposition for the model problem. In section 3, the discretization schemes for the physical problem will be derived in detail. In section 4, several numerical examples are given to demonstrate the numerical efficiency and accuracy of our method. The conclusions are presented in the last section.

2 Moving mesh method in conjunction with domain decomposition

In the last decade, moving mesh method in conjunction with a Schwarz domain decomposition has been developed by Haynes and his co-workers (see i.e. [22, 23] and references therein). And in this section, we will introduce a slight different method, that is, moving mesh method in conjunction with a non-overlapping domain decomposition.

Denote the observed domain by $[x_l, x_r]$ and assume it containing all sources, that is, $x_l < \alpha_0(t) < \alpha_1(t) < \dots < \alpha_{q-1}(t) < x_r$. Here x_l, x_r are either constants or variables of t . Then, the observed domain is divided into $q + 1$ subdomains $[\alpha_{i-1}, \alpha_i]$ ($i = 0, 1, \dots, q$) with $\alpha_{-1} = x_l, \alpha_q = x_r$, by the q sources respectively. Obviously, the sizes of the subdomains are variables of t too.

Let x and ξ denote physical and computational coordinates, respectively. Without loss of generality we assume the computational domain is $[0, 1]$. Then an one-to-one coordinate transformation between the observed domain $[x_l, x_r]$ and the computational domain $[0, 1]$ is defined by

$$x = x(\xi, t), \quad \xi \in [0, 1], \quad (6)$$

with

$$x(0, t) = x_l, \quad x(1, t) = x_r.$$

For a given uniform mesh, $\xi_j = \frac{j}{N}, j = 0, 1, \dots, N$, on the computational domain, the corresponding mesh on the observed domain $[x_l, x_r]$ is

$$x_l = x_0(t) < x_1(t) < \dots < x_{N-1}(t) < x_N(t) = x_r.$$

In our method, the coordinate transformation (6) is determined as a piecewise smooth function. On each subdomain $[\alpha_{i-1}, \alpha_i]$, $i = 0, 1, \dots, q$, it is the solution of an MMPDE which is derived from the equidistribution principle. In the literature, the following MMPDEs

$$\frac{\partial}{\partial \xi} \left(M \frac{\partial \dot{x}}{\partial \xi} \right) = -\frac{1}{\tau} \frac{\partial}{\partial \xi} \left(M \frac{\partial x}{\partial \xi} \right), \quad (7)$$

$$-\dot{x} = -\frac{1}{\tau} \frac{\partial}{\partial \xi} \left(M \frac{\partial x}{\partial \xi} \right), \quad (8)$$

$$\frac{\partial^2 \dot{x}}{\partial \xi^2} = -\frac{1}{\tau} \frac{\partial}{\partial \xi} \left(M \frac{\partial x}{\partial \xi} \right), \quad (9)$$

which known as MMPDE4, MMPDE5 and MMPDE6, respectively, are popularly used after they were originally established and analyzed in [14]. Here $M = M(x, t)$ is the monitor function giving some measure of the solution error on the physical domain and $\tau > 0$ is a parameter representing a timescale for adjusting the mesh toward equidistribution. In the asymptotic case $t \rightarrow \infty$, the solution of MMPDE4, MMPDE5 and MMPDE6 would satisfy the equidistribution principle, which is stated that [14]

$$\frac{\partial}{\partial \xi} \left(M \frac{\partial x}{\partial \xi} \right) = 0. \quad (10)$$

For more details about MMPDE, one can refer to [14] or the recent book [16]. In this paper, MMPDE6 (9) with the boundary condition

$$x(\xi_{j_{i-1}^s}, t) = \alpha_{i-1}(t), \quad x(\xi_{j_i^s}, t) = \alpha_i(t), \quad i = 0, 1, \dots, q, \quad (11)$$

is employed as an example to describe our moving mesh strategy in conjunction with domain decomposition. Here j_i^s is some fixed index satisfying $0 < j_i^s < N$. The resulting mesh, used to solve the model problem on $[x_l, x_r]$, satisfies the property that a fixed mesh point is located on each source during the time in consideration, i.e. $x_{j_i^s} \equiv \alpha_i(t)$.

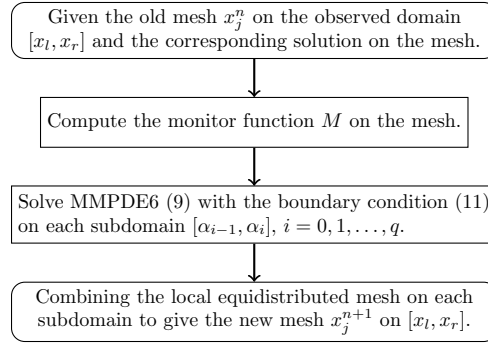


Figure 1: The moving mesh strategy in conjunction with domain decomposition.

Figure 1 shows the moving mesh strategy in conjunction with domain decomposition. Here the computation of the monitor function will be presented in section 4. And MMPDE6 (9) is solved by the following finite difference scheme

$$\frac{(x_{j+1}^{n+1} - 2x_j^{n+1} + x_{j-1}^{n+1}) - (x_{j+1}^n - 2x_j^n + x_{j-1}^n)}{\Delta t_n} = -\frac{1}{\tau} \left(M_{j+\frac{1}{2}}(x_{j+1}^{n+1} - x_j^{n+1}) - M_{j-\frac{1}{2}}(x_j^{n+1} - x_{j-1}^{n+1}) \right) \quad (12)$$

in our numerical examples, where $\Delta t_n = t_{n+1} - t_n$ and $M_{j+\frac{1}{2}} = (M_{j+1} + M_j)/2$.

The new mesh could be obtained very efficiently by parallel computing based on domain decomposition methods [21]. And it is best in the sense of equidistribution on each subdomain. On the other hand, we will found in the next section that the computation of the jump $[u]$ is avoided, hence the discretization scheme for the physical PDE (1) becomes very simple.

3 Model discretization and final algorithm

In this section, we derive the discretization schemes for the physical model problem (1)–(3) and (4) on the observed domain $[x_l, x_r]$ with appropriate boundary conditions. Then present a full algorithm of moving mesh method for the model problem.

3.1 Discretization schemes

For an arbitrary function $f = f(x, t) = f(x(\xi, t), t)$, we have

$$\dot{f} = \frac{\partial f}{\partial t}(x(\xi, t), t) \Big|_{\xi \text{ fixed}} = f_t + f_x \dot{x}.$$

Through the coordinate transformation (6), we can rewrite equation (1) on the computational coordinates as

$$\dot{u} - u_x \dot{x} - u_{xx} = \sum_{i=0}^{q-1} F_i(t, x, u) \delta(x - \alpha_i(t)). \quad (13)$$

Since the right-hand side of (13) vanishes when $x \neq \alpha_i(t)$, that is,

$$\dot{u} - u_x \dot{x} - u_{xx} = 0, \quad (14)$$

we conduct the discretization scheme for (13) on the above equation as [19], with each term on the left-hand side of (14) containing the information of jumps when they cross the sources. Physically, the value u of i th source changes smoothly as time evolution, which means the jump of the directional derivative of $u(x, t)$ along the vector $(\alpha'_i(t), 1)$ is zero [4, 19], i.e.,

$$[u_t]_{(\alpha_i(t), t)} + [u_x]_{(\alpha_i(t), t)} \alpha'_i(t) = 0, \quad i = 0, 1, \dots, q-1. \quad (15)$$

Recalling that $x_{j_i^s} \equiv \alpha_i(t)$, it follows that

$$[\dot{u}]_{(\alpha_i(t), t)} = [u_t + u_x \dot{x}]_{(\alpha_i(t), t)} = [u_t]_{(\alpha_i(t), t)} + \dot{x} [u_x]_{(\alpha_i(t), t)} = 0, \quad i = 0, 1, \dots, q-1. \quad (16)$$

By using the above equation, we can deduce from (14) that

$$[u_{xx}]_{(\alpha_i(t), t)} = [\dot{u} - u_x \dot{x}]_{(\alpha_i(t), t)} = [\dot{u}]_{(\alpha_i(t), t)} - \dot{x} [u_x]_{(\alpha_i(t), t)} = -\alpha'_i(t) [u_x]_{(\alpha_i(t), t)}, \quad (17)$$

$i = 0, 1, \dots, q-1$. Then we obtain immediately

$$[u_{xx}]_{(\alpha_i(t), t)} = \psi_i(t, \alpha_i(t), u) F_i(t, \alpha_i(t), u(\alpha_i(t), t)), \quad i = 0, 1, \dots, q-1, \quad (18)$$

by taking (4) and (5) into (17).

Similarly to [19], the discretization scheme for (13) are divided into two cases due to $x_{j_i^s} \equiv \alpha_i(t)$ during time integration. For $j \neq j_i^s$, $i = 0, 1, \dots, q-1$, the mesh point not located at the source, (13)

is discretized by standard center difference for spatial variable and backward difference for temporal variable, that is,

$$\frac{u_j^{n+1} - u_j^n}{\Delta t_n} - \frac{u_{j+1}^{n+1} - u_{j-1}^{n+1}}{h_{j+1}^{n+1} + h_j^{n+1}} \left(\frac{x_j^{n+1} - x_j^n}{\Delta t_n} \right) - \frac{2}{h_{j+1}^{n+1} + h_j^{n+1}} \left(\frac{u_{j+1}^{n+1} - u_j^{n+1}}{h_{j+1}^{n+1}} - \frac{u_j^{n+1} - u_{j-1}^{n+1}}{h_j^{n+1}} \right) = 0, \quad (19)$$

where $h_j^n = x_j^n - x_{j-1}^n$. Here x_j^n, u_j^n are the mesh and the solution on it at time step t_n , respectively. For $j = j_i^s$, the mesh point just located at the source, the jump informations should be incorporated into the discretization scheme. For this case, the discretization scheme for (13) reads

$$\begin{aligned} \frac{u_{j_i^s}^{n+1} - u_{j_i^s}^n}{\Delta t_n} - \frac{u_{j_i^s+1}^{n+1} - u_{j_i^s-1}^{n+1}}{h_{j_i^s+1}^{n+1} + h_{j_i^s}^{n+1}} \psi_i^{n+1} - \frac{2}{h_{j_i^s+1}^{n+1} + h_{j_i^s}^{n+1}} \left(\frac{u_{j_i^s+1}^{n+1} - u_{j_i^s}^{n+1}}{h_{j_i^s+1}^{n+1}} - \frac{u_{j_i^s}^{n+1} - u_{j_i^s-1}^{n+1}}{h_{j_i^s}^{n+1}} \right) \\ - \frac{2}{h_{j_i^s+1}^{n+1} + h_{j_i^s}^{n+1}} F_i(u_{j_i^s}^{n+1}) = 0, \end{aligned} \quad (20)$$

where $\psi_i^{n+1} \approx \psi_i(t_{n+1}, \alpha_i^{n+1}, u^{n+1})$, $F_i(u_{j_i^s}^{n+1}) \approx F_i(t_{n+1}, \alpha_i^{n+1}, u_{j_i^s}^{n+1})$, $i = 0, 1, \dots, q-1$.

In the above schemes, we need the source position $\alpha_i(t_{n+1})$ at time step t_{n+1} . For the general movement (4), it is computed by the following Crank-Nicolson scheme

$$\alpha_i^{n+1} = \alpha_i^n + \frac{\Delta t_n}{2} (\psi_i^{n+1} + \psi_i^n), \quad i = 0, 1, \dots, q-1, \quad (21)$$

as in [20]. If $\psi_i(t, \alpha_i(t), u)$, $i = 0, 1, \dots, q-1$, are independent of u , the source position α_i^{n+1} and the speed ψ_i^{n+1} can be calculated in advance before solving the discretization schemes for MMPDE6 (9) and physical PDE (13). Otherwise, the resulting system would be too complicated to be solved. In this case, we decouple the discretization system by a predictor-corrector algorithm. For the predictor step, assume $\psi_i^{n+1} = \psi_i^n$ and solve (21) to get an approximate variable α_i^* of α_i^{n+1} . Then substituting ψ_i^{n+1} and α_i^* into the discretization schemes for (9) and (13) to obtain an approximate solution u^* of u^{n+1} . For the corrector step, compute $\psi_i^{n+1} = \psi_i(t_{n+1}, \alpha_i^*, u^*)$ and solve (21) to get α_i^{n+1} , then obtain the solution u^{n+1} at time step t_{n+1} by the discretization schemes for (9) and (13).

To complete the discretization schemes, we require an appropriate condition for u on the boundary of the observed domain $[x_l, x_r]$. For the observed domain is small enough, we employ a third-order local absorbing boundary condition (LABC) proposed in [24]

$$3s_0 u_x + u_{xt} \pm s_0 \sqrt{s_0} u \pm 3\sqrt{s_0} u_t = 0 \quad (22)$$

for (1) as in [19, 20]. Here s_0 is a user-defined parameter, the plus sign in " \pm " corresponds to the LABC at the right boundary x_r , and the minus sign corresponds to the one at the left boundary x_l . Under the map (6), we get the LABC for (13) as follows

$$\dot{u}_x \pm 3\sqrt{s_0} \dot{u} + 3s_0 u_x - u_{xx} \dot{x} \pm s_0 \sqrt{s_0} u \pm (-3\sqrt{s_0} u_x \dot{x}) = 0, \quad (23)$$

where the plus sign in " \pm " corresponds to the right boundary, and the minus sign corresponds to

the left boundary. According to [19, 20], a finite difference scheme for (23) is

$$\begin{aligned} & \frac{1}{\Delta t_n} \left(\frac{u_1^{n+1} - u_{-1}^{n+1}}{2h_1^{n+1}} - \frac{u_1^n - u_{-1}^n}{2h_1^n} \right) - 3\sqrt{s_0} \frac{u_0^{n+1} - u_0^n}{\Delta t_n} + 3 \left(s_0 + \sqrt{s_0} \frac{x_0^{n+1} - x_0^n}{\Delta t_n} \right) \frac{u_1^{n+1} - u_{-1}^{n+1}}{2h_1^{n+1}} \\ & - \left(\frac{x_0^{n+1} - x_0^n}{\Delta t_n} \right) \frac{u_1^{n+1} - 2u_0^{n+1} + u_{-1}^{n+1}}{(h_1^{n+1})^2} - s_0 \sqrt{s_0} u_0^{n+1} = 0, \end{aligned} \quad (24)$$

on the left boundary, and

$$\begin{aligned} & \frac{1}{\Delta t_n} \left(\frac{u_{N+1}^{n+1} - u_{N-1}^{n+1}}{2h_N^{n+1}} - \frac{u_{N+1}^n - u_{N-1}^n}{2h_N^n} \right) + 3\sqrt{s_0} \frac{u_N^{n+1} - u_N^n}{\Delta t_n} + 3 \left(s_0 - \sqrt{s_0} \frac{x_N^{n+1} - x_N^n}{\Delta t_n} \right) \frac{u_{N+1}^{n+1} - u_{N-1}^{n+1}}{2h_N^{n+1}} \\ & - \left(\frac{x_N^{n+1} - x_N^n}{\Delta t_n} \right) \frac{u_{N+1}^{n+1} - 2u_N^{n+1} + u_{N-1}^{n+1}}{(h_N^{n+1})^2} + s_0 \sqrt{s_0} u_0^{n+1} = 0. \end{aligned} \quad (25)$$

on the right boundary. Here two ghost points x_{-1} and x_{N+1} are used. On the other hand, if the observed domain is big enough or else, Dirichlet boundary conditions are employed.

3.2 Full algorithm

We close this section with a full algorithm in Figure 2 for the model problem (1)–(3) and (4). Here the choice of the time step Δt_n will be determined in the following concrete examples, and $Tol > 0$ is set to be 10^{-16} .

4 Numerical examples

In this section, we present some numerical examples to verify the convergence rate and illustrate efficiency of the full algorithm in Figure 2.

Example 1. *We consider a nonlinear moving interface problem with the following exact solution*

$$u(x, t) = \begin{cases} \sin(\omega_1 x) e^{-\omega_1^2 t}, & x \leq \alpha_0(t), \\ \sin(\omega_2(1 - x)) e^{-\omega_2^2 t}, & x \geq \alpha_0(t), \end{cases} \quad (26)$$

for some choice of ω_1 and ω_2 . The interface $\alpha_0(t)$ is determined by solving the scalar equation

$$\sin(\omega_1 \alpha_0) e^{-\omega_1^2 t} = \sin(\omega_2(1 - \alpha_0)) e^{-\omega_2^2 t}, \quad (27)$$

so that $u(x, t)$ is continuous across the interface.

The equation (27) has a unique solution on $[0, 1]$ if we take, for example, $\pi < \omega_1$, $\omega_2 < 2\pi$. Then we have the ordinary differential equation for the motion of the interface

$$\frac{d\alpha_0}{dt} = \frac{(\omega_1^2 - \omega_2^2)u(\alpha_0, t)}{u_x(\alpha_0^-, t) - u_x(\alpha_0^+, t)}. \quad (28)$$

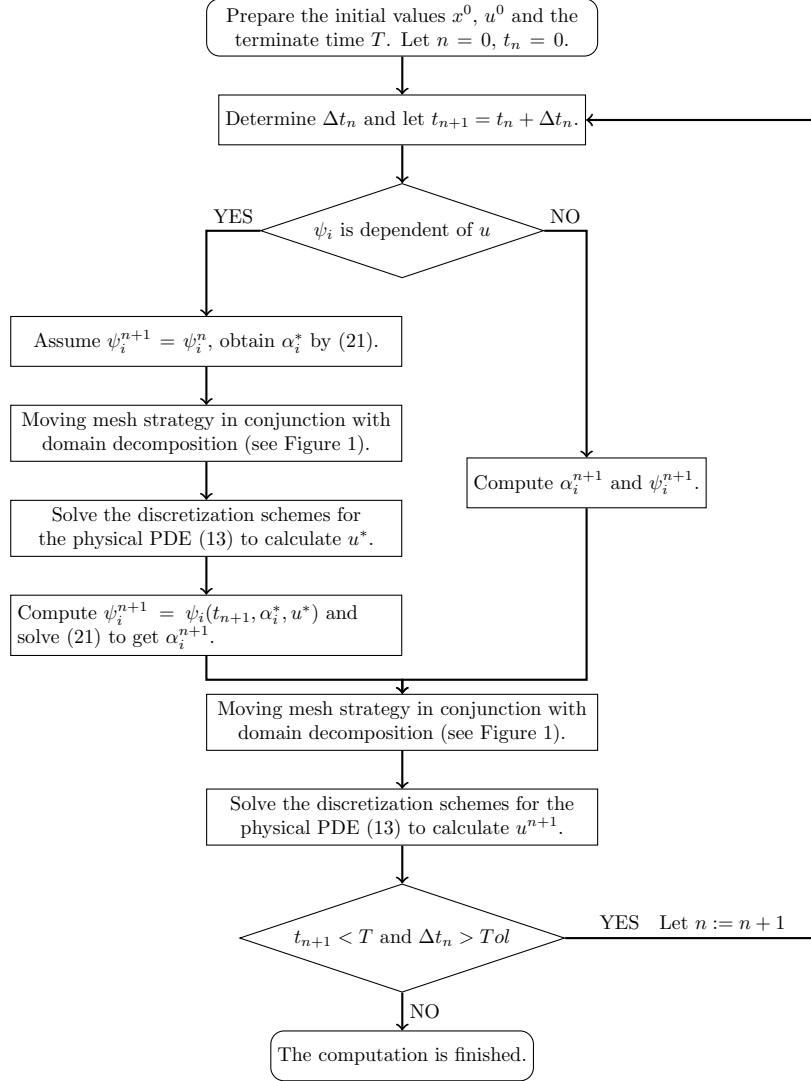


Figure 2: Full algorithm for numerical solution of the model problem (1)-(4).

Based on the jump conditions, the source function $F_0(t, x, u)$ is

$$\begin{aligned}
 F_0(t, x, u) &= -[u_x]_{\alpha_0} = u_x(\alpha_0^-, t) - u_x(\alpha_0^+, t) \\
 &= \omega_1 \cos(\omega_1 \alpha_0) e^{-\omega_1^2 t} + \omega_2 \cos(\omega_2 (1 - \alpha_0)) e^{-\omega_2^2 t}.
 \end{aligned} \tag{29}$$

Same as in [2], we take $\omega_1 = 5\pi/4$, $\omega_2 = 7\pi/4$. The observed domain is set by $[0, 1]$, where the initial position of the interface is $\alpha_0(0) = 0.58333$. Since we have the exact solution, Dirichlet boundary conditions are employed. In this example, we simply use the uniform time step, i.e. $\Delta t_n \equiv \text{const}$, and the total number of the time meshes is L . The monitor function for MMPDE6 (9) takes the

form

$$M(x, t) = (1 - \theta) \left| \frac{\partial u}{\partial x} \right| + \theta ((x - \alpha_0(t))^2 + \varepsilon)^{-1/4}, \quad (30)$$

where $0 < \theta < 1$, $0 < \varepsilon \ll 1$. This is consistent with the choice in [19, 20]. In practice, smoothing the monitor function can improve the accuracy of the numerical solution, and we utilize the smoothing technique proposed in [25]. Here the parameters in MMPDE6 (9) and the monitor function (30) are given by $\tau = 10^{-3}$, $\theta = 0.5$, and $\varepsilon = 10^3/N^4$.

Since backward Euler scheme is used to solve the physical PDE in this paper, the truncation error for time discretization is only first-order. To verify our algorithm has a second-order convergence rate for space, the number of L should be fourfold when N is double in the convergence test. Computational results with different number of N and L at the time $T = 0.1$ are listed in Table 1, where the errors are defined as

$$E_{N,L} = \|U - u_e\|_{\infty}, \quad \tilde{E}_{N,L} = \|\tilde{U} - u_e\|_{\infty}, \quad E_{N,L}^{\alpha} = |\tilde{\alpha}_0 - \alpha_0^*|.$$

Here, u_e is the true solution, α_0^* used as the exact interface is the solution of a zero-finding MATLAB function *fzero* for (27). The numerical solution U is obtained by the algorithm where $\alpha_0(t)$ and $\alpha_0'(t)$ are exactly calculated. And \tilde{U} , $\tilde{\alpha}_0$ represent respectively the numerical solution and interface, solved with the full predictor-corrector algorithm. The ratios in Table 1 are $E_{2N,4L}/E_{N,L}$, $\tilde{E}_{2N,4L}/\tilde{E}_{N,L}$ and $E_{2N,4L}^{\alpha}/E_{N,L}^{\alpha}$, respectively. It is shown that our algorithm solves the solution and the interface very well, and has a second-order convergence rate for space, i.e. $O(1/N^2)$. Additionally, compared the corresponding results in [3], our algorithm is better than the method proposed in [3].

Table 1: Error and convergence rates at $T = 0.1$.

N, L	$E_{N,L}$	ratio	$\tilde{E}_{N,L}$	ratio	$E_{N,L}^{\alpha}$	ratio
40, 40	1.0931e-2	-	1.3721e-2	-	8.2720e-3	-
80, 160	2.6996e-3	0.24697	3.3908e-3	0.24713	2.0540e-3	0.24830
160, 640	6.6945e-4	0.24798	8.4144e-4	0.24816	5.1038e-4	0.24848
320, 2560	1.6687e-4	0.24927	2.0981e-4	0.24935	1.2732e-4	0.24947
640, 10240	4.1678e-5	0.24976	5.2408e-5	0.24978	3.1807e-5	0.24982
1280, 40960	1.0416e-5	0.24992	1.3098e-5	0.24993	7.9500e-6	0.24994
2560, 163840	2.6038e-6	0.24998	3.2743e-6	0.24998	1.9874e-6	0.24998

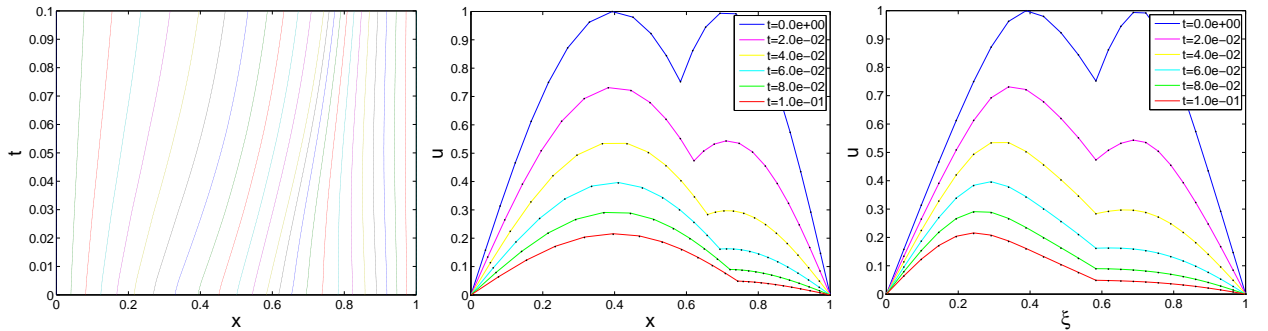


Figure 3: Mesh trajectories and the profiles of u in physical variable and computational variable (from left to right) as time changes with $N = 24$. The solid lines are the computed solution and the dots are the exact solution on the mesh.

Figure 3 presents the profiles of the solution in physical variable and computational variable and the evolving mesh from $t = 0$ to $t = 0.1$. The number of the mesh is $N = 24$, with half mesh points on each side of the interface. We can see that we get excellent resolution of the example even with a grid as coarse as $N = 24$.

The rest examples are from traveling heat sources problems with the solution may be blow-up [4, 17, 19, 20]. If not specifically pointed out, the initial value is given by

$$u(x, 0) = \begin{cases} \cos^2(\pi x/2), & -1 < x < 1, \\ 0, & \text{otherwise,} \end{cases} \quad (31)$$

the observed domain is set by $[-10, 10]$ with $u(-10, t) = u(10, t) = 0$, and the source functions $F_i(t, x, u)$ are simply specified by

$$F_i(t, x, u) = 1 + u^2, \quad i = 0, 1, \dots, q-1. \quad (32)$$

The resulting nonlinear system is solved by Newton iteration with the tolerance $tol = 10^{-8}$.

The monitor function for MMPDE6 (9) takes the form

$$M(x, t) = \theta_{q+1}u^p + \theta_q \left| \frac{\partial u}{\partial x} \right| + \sum_{i=0}^{q-1} \theta_i ((x - \alpha_i(t))^2 + \varepsilon)^{-1/4}, \quad (33)$$

where the parameters $0 < \theta_i < 1$, $\sum_{i=0}^{q+1} \theta_i = 1$, $0 < \varepsilon \ll 1$, $p > 0$ will be determined later. For non-blow-up case, the following graded time steps [4, 17]

$$t_n = \left(n \frac{T}{L} \right)^2, \quad n = 0, 1, \dots, L,$$

are used with $[0, T]$ the time integration interval and L the number of time meshes. While for blow-up case, the time step $\Delta t_n = t_{n+1} - t_n$ is chosen to be [4, 26]

$$\Delta t_n = \min \left\{ \mu, \frac{\mu}{\left(\max_j \{u_j^n\} + \varepsilon \right)^2} \right\},$$

where ε is same in the monitor function, μ is a small positive constant with $\mu = 10^{-3}$ in the test.

Example 2 (Linear moving sources). *We consider that all sources move with a constant velocity k , and the position of the i -th source has a constant distance d_i to the 0-th source, i.e.,*

$$\alpha'_i(t) = k, \quad \alpha_i(0) = d_i, \quad i = 0, 1, \dots, q-1,$$

where $d_0 = 0$.

Since our method is trivial for multi-sources case, only $q = 1, 2$ are considered. Different velocities k are investigated in [4, 17, 19] and we specify $k = 2$ here. With this velocity, blow-up would occur for $q = 2$, and be avoided for $q = 1$. The parameters are set by $\tau = 10^{-3}$, $\theta_0 = 0.9$, $\theta_1 = 0.1$, and $\varepsilon = 10^3/N^4$ for $q = 1$, while $\tau = 5 \times 10^{-4}$, $\theta_0 = \theta_1 = 0.3$, $\theta_3 = 0.4$, $p = 2$, $\varepsilon = 10^{-5}$, and $d_1 = 2.5$ for $q = 2$, respectively.

The profiles of the computed solution in physical variable and computational variable and the evolving mesh are presented in Figure 4 for $q = 1$ and in Figure 5 for $q = 2$. For simplicity, each subdomain has 50 mesh points, i.e. $N = 100$ for $q = 1$ and $N = 150$ for $q = 2$. The numerical results are coincide with that in [4, 17], and the blow-up time is 2.039708648680643 at the first source $x = 4.079417297361286$, corresponding to the maximum value of $u_{\max} = 3.16 \times 10^6$.

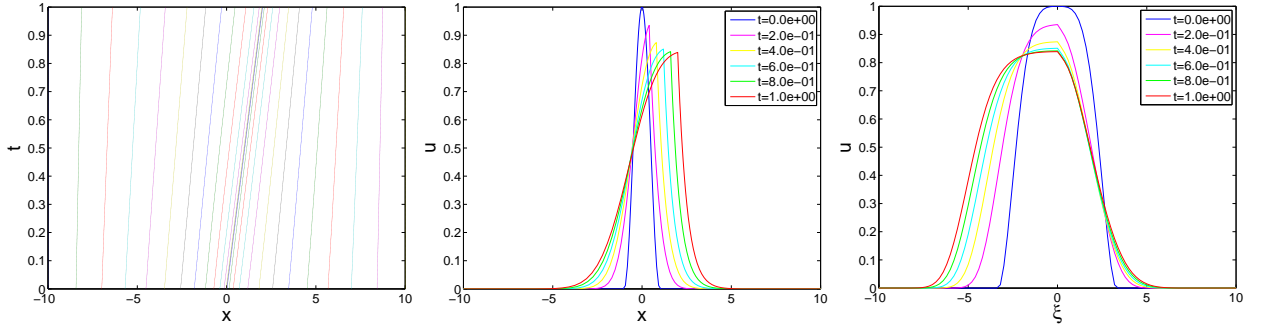


Figure 4: Mesh trajectories and the profiles of u from $t = 0$ to $t = 1.0$ for one source case with $N = 100$.

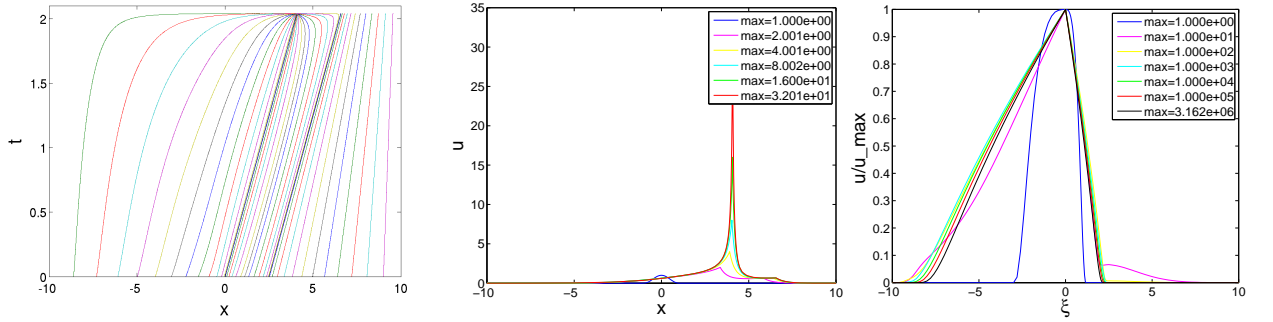


Figure 5: Mesh trajectories and the profiles of u for two sources case with $N = 150$.

Example 3 (Sin-type moving sources). *We now consider two sources case, in which the sources move periodically with the same speed while separated by a constant distance $d_1 = 2.5$, that is,*

$$\alpha'_0(t) = \alpha'_1(t) = A \cos(\pi t), \quad \alpha_0(0) = 0.$$

The Blow-up phenomenon is studied in [19] for different amplitudes A . Here we only give the numerical results for $A = \pi$ (see Figure 6), since all results are similar to those in [19]. All parameters are chosen the same as those in last example. The blow-up occurs at $t = 1.689611393639939$ on the second source with the maximum value of $u_{\max} = 3.16 \times 10^6$.

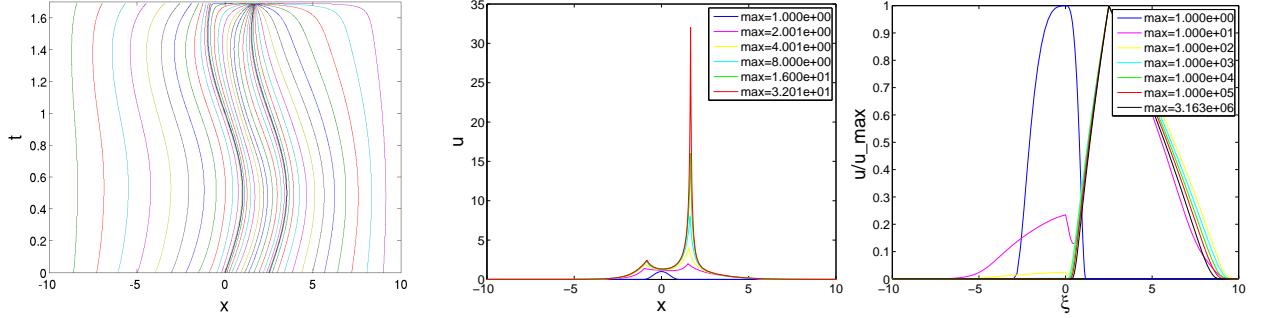


Figure 6: Mesh trajectories and the profiles of u for $q = 2$, $A = \pi$ with $N = 150$.

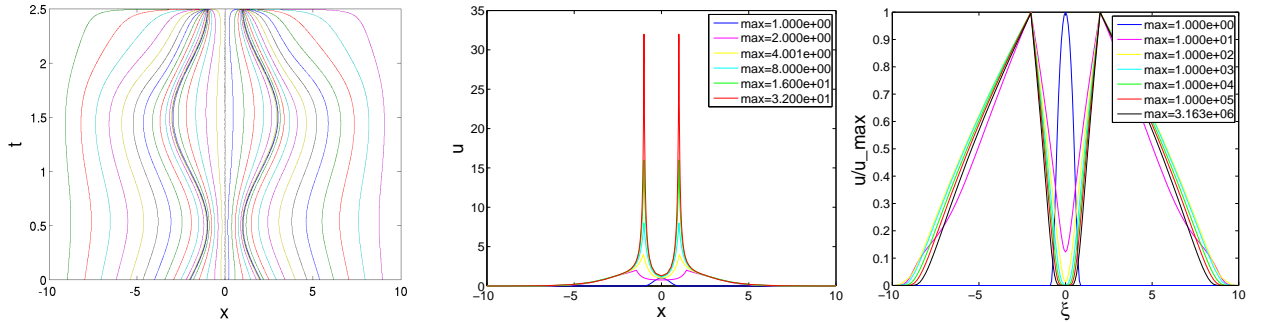


Figure 7: Numerical results for symmetric periodic moving sources with $N = 150$.

Example 4 (Symmetric periodic moving sources). *We consider the case for two sources, which move periodically and symmetrically. The motion are described by*

$$\alpha'_0(t) = A \cos(\pi t), \quad \alpha_0(0) = -2.0,$$

and $\alpha_1(t) = -\alpha_0(t)$, with e.g. $A = \pi$.

To our best knowledge, there has no theoretical results for multi-sources with different speeds and this is the first time numerically investigating the phenomenon for this case. It is shown in Figure 7 that blow-up occurs on both sources at $t = 2.496881990359248$, corresponding to the maximum value of $u_{\max} = 3.16 \times 10^6$.

If local absorbing boundary conditions (23) are used, the observed domain can be chosen more smaller while the results do not be influenced almost. See Figure 8 as an example, where the observed domain is set by $[\alpha_0(t) - 4.0, \alpha_1(t) + 4.0]$, changed as time evolution. Now blow-up occurs on both sources at $t = 2.496370241342059$ with the maximum value of $u_{\max} = 3.16 \times 10^6$.

5 Conclusions

In this paper, our work focus on the problem of traveling singular sources with different speeds. A new moving mesh method in conjunction with a non-overlapping domain decomposition is proposed

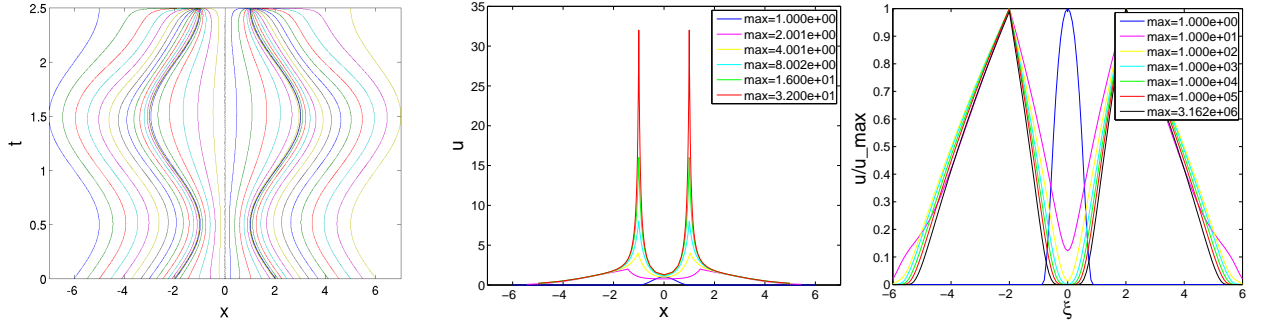


Figure 8: Numerical results for symmetric periodic moving sources with $[x_l, x_r] = [\alpha_0(t) - 4.0, \alpha_1(t) + 4.0]$.

for solving this problems. The whole domain is splitted into $q + 1$ subdomains by the q sources, whose positions are gotten by a predictor-corrector algorithm. Taking the advantages of the domain decomposition, the computation of jump $[u]$ is avoided and there are only two different cases discussed in the discretization of the physical PDE. Thus, it is easy for the implementation to solve the problems with two traveling sources or more. Moreover, the moving mesh method of MMPDEs can be applied into each sub-domain respectively. The second-order of the spatial convergence can be proved for the new method under a special time marching implementation. The good performance of the new method for the blow-up phenomenon is demonstrated through a number of examples with two sources. Furthermore, using the new method, we successfully simulate the solutions of two sources with different speeds. To our best knowledge, this is the first time investigation for this case. The case of three sources or more can be implemented similarly.

Acknowledgment

This work was partially supported by a grant of key program from the National Natural Science Foundation of China (No. 10731060, 10801120, 11171305), National Basic Research Program of China (2011CB309704), Chinese Universities Scientific Fund No. 2010QNA3019 and Zhejiang Provincial Natural Science Foundation of China under Grant No. Y6110252.

References

- [1] C. M. Kirk and W. E. Olmstead. Blow-up in a reactive-diffusive medium with a moving heat source. *Zeitschrift für angewandte Mathematik und Physik*, 53(1):147–159, 2002.
- [2] R. P. Beyer and R. J. LeVeque. Analysis of a one-dimensional model for the immersed boundary method. *SIAM Journal on Numerical Analysis*, 29(2):332–364, 1992.
- [3] Z. Li. Immersed interface methods for moving interface problems. *Numerical Algorithms*, 14(4):269–293, 1997.
- [4] J. Ma and Y. Jiang. Moving mesh methods for blowup in reaction-diffusion equations with traveling heat source. *Journal of Computational Physics*, 228(18):6977–6990, 2009.

- [5] P. Smereka. The numerical approximation of a delta function with application to level set methods. *Journal of Computational Physics*, 211(1):77–90, 2006.
- [6] R. J. LeVeque and Z. Li. The immersed interface method for elliptic equations with discontinuous coefficients and singular sources. *SIAM Journal on Numerical Analysis*, 31(4):1019–1044, 1994.
- [7] Juri D. Kandilarov. Immersed interface method for a reaction-diffusion equation with a moving own concentrated source. In Ivan Dimov, Ivan Lirkov, Svetozar Margenov, and Zahari Zlatev, editors, *Numerical Methods and Applications*, volume 2542 of *Lecture Notes in Computer Science*, pages 506–513. Springer-Verlag Berlin Heidelberg, 2003.
- [8] X. Yang, X. Zhang, Z. Li, and G. W. He. A smoothing technique for discrete delta functions with application to immersed boundary method in moving boundary simulations. *Journal of Computational Physics*, 228(20):7821–7836, 2009.
- [9] C. S. Peskin. Numerical analysis of blood flow in the heart. *Journal of Computational Physics*, 25(3):220–252, 1977.
- [10] W. E. Olmstead. Critical speed for the avoidance of blow-up in a reactive-diffusive medium. *Zeitschrift für angewandte Mathematik und Physik*, 48(5):701–710, 1997.
- [11] C. M. Kirk and W. E. Olmstead. The influence of two moving heat sources on blow-up in a reactive-diffusive medium. *Zeitschrift für angewandte Mathematik und Physik*, 51(1):1–16, 2000.
- [12] C. J. Budd, W. Huang, and R. D. Russell. Moving mesh methods for problems with blow-up. *SIAM Journal on Scientific Computing*, 17(2):305–327, 1996.
- [13] W. Huang, J. Ma, and R. D. Russell. A study of moving mesh PDE methods for numerical simulation of blowup in reaction diffusion equations. *Journal of Computational Physics*, 227(13):6532–6552, 2008.
- [14] W. Huang, Y. Ren, and R. D. Russell. Moving mesh partial differential equations (MMPDES) based on the equidistribution principle. *SIAM Journal on Numerical Analysis*, 31(3):709–730, 1994.
- [15] T. Tang and J. Xu. *Adaptive Computations: Theory and Algorithms*. Science Press, Beijing, 2007.
- [16] W. Z. Huang and R. D. Russell. *Adaptive Moving Mesh Methods*. Springer Science+Business Media, LLC, 2011.
- [17] H. Zhu, K. Liang, and X. Cheng. A numerical investigation of blow-up in reaction-diffusion problems with traveling heat sources. *Journal of Computational and Applied Mathematics*, 234:3332–3343, 2010.
- [18] H. Zhu and K. Liang. Moving mesh method for a reaction-diffusion equation with traveling heat source on unbounded domain. submitted, 2010.

- [19] Z. Hu, K. Liang, and H. Zhu. A moving mesh method for reaction-diffusion equations with traveling heat sources on unbounded domains. *Applied Numerical Mathematics*, under review, 2011.
- [20] Z. Hu and H. Wang. A moving mesh method for heat equation with traveling singular sources (in chinese). *Applied Mathematics. A Journal of Chinese Universities. Ser. A*, 2012. accepted.
- [21] A. Toselli and O. B. Widlund. *Domain Decomposition Methods - Algorithms and Theory*. Springer-Verlag, Berlin, 2005.
- [22] R. D. Haynes and R. D. Russell. A Schwarz waveform moving mesh method. *SIAM Journal on Scientific Computing*, 29(2):656–673, 2007.
- [23] M. J. Gander and R. D. Haynes. Domain decomposition approaches for mesh generation via the equidistribution principle. *SIAM Journal on Numerical Analysis*, 50:2111–2135, 2012.
- [24] H. Brunner, X. Wu, and J. Zhang. Computational solution of blow-up problems for semilinear parabolic PDEs on unbounded domains. *SIAM Journal on Scientific Computing*, 31(6):4478–4496, 2010.
- [25] W. Huang, Y. Ren, and R. D. Russell. Moving mesh methods based on moving mesh partial differential equations. *Journal of Computational Physics*, 113(2):279–290, 1994.
- [26] C. J. Budd, B. Leimkuhler, and M. D. Piggott. Scaling invariance and adaptivity. *Applied Numerical Mathematics*, 39:261–288, 2001.